2013 Brazilian Power Electronics Conference (COBEP)

IEEE Catalog Number: CFP1377F-USB • ISBN: 978-1-4799-0270-5

COBEP 2013

XII Brazilian Power Electronics Conference

Serra Azul Hotel - Gramado - RS / Brazil From 27 to 31 October

PROCEEDINGS

DIGITALLY IMPLEMENTED NATURALLY SAMPLED SVM APPLIED IN SPEED SENSOR-LESS FIELD ORIENTED CONTROLLED INDUCTION MOTOR DRIVE

Péter Stumpf*‡, Rafael K. Járdán†, István Nagy†‡
*Budapest University of Technology and Economics, Department of Mechatronics, Optics and Engineering Informatics
†Budapest University of Technology and Economics, Department of Automation and Applied Informatics
‡MTA-BME Control Engineering Research Group
Budapest, Hungary, e-mail: *stumpf@get.bme.hu*

***Abstract*—One possible implementation form of Space Vector Modulation is the Naturally Sampled (NS) one. Its favourable properties are that no distortion or delayed response are introduced by it. The aim of the paper is to introduce a digital method to implement NS SVM and compares its performance with the widely applied Regular and Doublesampled modulation form in a closed-loop speed sensor-less motor drive system. The paper focuses on the case when both the sampling over reference frequency ratio F and the carrier over reference frequency m_f is low. The investigation covers two widely applied current measurement techniques.**

***Keywords*—PWM converter issues, Sensorless Drive, Induction Machine**

I. INTRODUCTION

The high speed drives poses many challenges not only in the field of electric motor design [1], but also in the field of industrial electronics. The two basic divisions of industrial electronics, power electronics and digital signal processing play a decisive role in the development and the appearance of high performance ultrahigh speed motor drives [2]. In a modern closed loop controlled high speed drive systems, all the signal processes including the speed and current regulation loop and also the PWM block are implemented in the digital domain. Even with the up-to-date digital devices with clock frequency in the range of tens of MHz, the sampling frequency (f_s) is limited. As a results the ratio of the sampling frequency and the actual fundamental frequency $F = f_s/f_1$ around the maximum speed of a high speed motor is also low, resulting in stability problems and sampling error in the regulation loop.

It should be noted, the problems encountered previously with the high speed drives appear also in high-pole count motor, used widely for hybrid and electric vehicles. As in this case the number of poles is 20 or higher, the required synchronous frequency f_1, similar to ultrahigh speed drives, is higher than 1 kHz, while the output speed few thousand rpm. Furthermore, in some high power application the carrier frequency f_c is kept at low value in order to reduce the switching losses resulting again low m_f. These application fields give also practical significance of the research work presented in this paper.

In [3] a complex proportional and integral controller with predictive active damping term is developed to stabilize the current loop, while a model-based error estimator is offered to compensate the sampling error. In [4] an enhanced stationary Proportional-Integrator (PI) technique is introduced to compensate the transport delay caused by the PWM process. The paper [5] analyzes the behavior of discrete-time current regulators for high-speed automotive drives and large-traction drives applying low sampling frequency. In [6] the speed sensor-less drive performance is investigated at high speeds, with very low sampling to fundamental frequency ratio focusing on the problems of the rotor flux estimators. Field-angle correction method for speed sensor-less induction machine drives applying Field Oriented Control is discussed in [7].

The main purpose of the investigation presented in the paper is to study the effect of the sampling technique of the SVM process on the performance of a digitally implemented vector controlled induction machine drive. The investigation covers two widely applied current measurement techniques.

II. SENSORLESS FIELD ORIENTED CONTROL

The principal aim of the Field Oriented Control (FOC) is to independently control the flux and torque in the induction machine, in a similar way to the control of a separately excited DC machine in order to fast change the torque [8], [2], [9]. As there is a *"strong trend to avoid mechanical motion (speed/position) sensors because it reduces cost and improves reliability and functionality of the drive system"* [2], the investigation focuses on a speed sensor-less drive.

The schematic block diagram of the speed sensor-less FOC can be seen on Fig.1. The rotating reference frame (RRF denoted by dq) is rotating at synchronous angular velocity $\omega_1 = 2\pi f_1$. In the rotating reference frame fixed to the rotor flux the three phase stator currents in space vector form can be viewed as two dc quantities in steady state. The d and q axis current components are the rotor flux and torque producing component, respectively. As the two current components are orthogonal to each other the rotor flux and the torque can be controlled independently.

As a speed sensor is missing (Fig.1) an estimator block is applied to determine the actual mechanical speed Ω_{est}, the synchronous angular velocity ω_1 and the flux angle ρ_{est}. The inputs of the Estimator block is the phase currents of the motor in the $\alpha-\beta$ stationary reference frame and the reference values v_α^*, v_β^* of the Space Vector Modulation block produced by the d and q axis PI current control blocks, respectively.

Figure 2 shows the block diagram of the estimator block used in the speed sensor-less FOC drive. The theoretical background and the detailed description can be found in more details in [9], [8], here we only refer to them.

978-1-4799-0272-9/13/$31.00 ©2013 IEEE

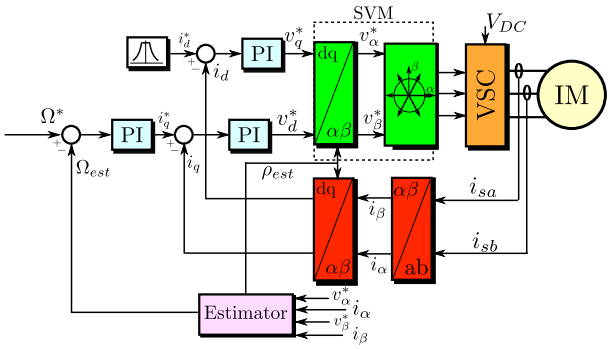

Fig. 1. Block diagram of the sensorless FOC

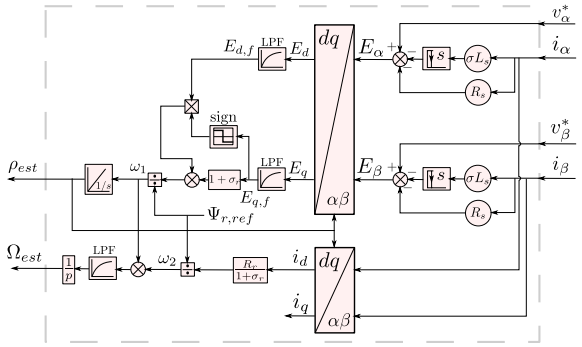

Fig. 2. Estimator block diagram

III. Current Sampling

As in modern high-performance closed loop drive systems, all the signal processes including the speed and current regulation loop and also the PWM block are implemented in the digital domain both the estimator presented in the continuous time domain and the continuous PI controllers must be discretized.

Generally the phase currents synchronously sampled at once or twice the carrier frequency to eliminate the current ripple without requiring low-pass filtering or complex ripple-elimination filters [10], [4]. Other reason to limit the sampling frequency is, it is advisory to update the duty ratio of the digital PWM module maximum twice during a carrier period to avoid intermediate PWM transitions and glitches in the switching signals.

The drawback of the solution is that the limited sampling frequency and the delay caused by the PWM module (see later) introduces a phase lag limiting the achievable control bandwidth and deteriorating the performance of the control loop. In general-purpose ac drive applications this effect can be neglected, but it can be crucial when both the sampling over reference frequency ratio F and the carrier over reference frequency m_f is low. In [11] a multisampling strategy is introduced for active filters by using FPGA. The disadvantage of the method is the required complex filter to eliminate the ripples in the current signal and the unwanted intermediate PWM transitions, which can be occur.

Another reason which determines the sampling frequency is the applied current sensing circuit. Generally two main methods are applied. In the first case by using a current transducer the output phase current signals can be continuously measured and there is no limitations regarding the sampling frequency.

Another solution is to apply a shunt resistor to measure the phase currents. It is a popular solution due to the low system cost and exact current measurement. The voltage across the resistor, which is proportional to the current, is filtered, shifted and finally amplified and fed to the AD module of the microcontrollers. In up-to-date IGBT power modules the current shunt resistors are placed directly on the printed circuit board. Several topologies can be used, but most often the resistor is placed on the bottom of the inverter legs. The drawback of the solution is that current flows across the resistor only when the lower switch conducts resulting a discontinuous current signal. By applying SVM and linear modulation all the three lower switches conduct at the maximum peak of the triangular carrier signal. It results that it is advisory to sample the phase currents at the the positive peaks of the carrier signal resulting in the sampling frequency has the same frequency as the carrier one $f_s = f_c$. Another topology when the resistors are placed in the output phases. The drawback of this solution is that the resistors are working at floating potential requiring a more complex isolated sensing circuitry. Later on we focus only on the case when the shunt resistor are placed in the bottom of the inverter leg.

Due to the losses in the current shunt resistor the application of shunt resistors are limited in the low power applications. However by placing the resistors as close as possible to the heat sink and use special precision shunt resistor the method are applied in medium and high power range, where mostly current transducers are utilised [12].

Figure 3a and 3b show the process of the digitally implemented speed sensor-less FOC by using shunt resistor and current transducer, respectively. In both case the current sampling is synchronized to the carrier signal. After measuring the stator currents in two phases the mechanical speed Ω_{est} and the angle ρ_{est} are estimated using the values obtained in the previous sampling period. Proportional integral controllers regulate the stator voltages in the $d-q$ frame by setting v_d^* and v_q^* to achieve the calculated reference stator currents i_d^* and i_q^*. The output signal of the controllers and the estimated flux angle ρ_{est} are the input signals for the Space Vector Modulation (SVM) block which calculates v_α^*, v_β^* and the reference signals $v_{ref,i}$ $(i = a, b, c)$ for each phase.

IV. Sampling of Space Vector Modulation

Three different Space Vector Modulation (SVM) sampling techniques used to be classified: Regular Sampling (RS), Natural Sampling (NS) and Oversampling (OS) [13]. Later on within the OS technique only the solution when the number of samples $n = 2$ (Doublesampling, DS) is discussed.

A. Digital Implementation of NS

As theoretically NS does not introduce distortion or a delayed response to the reference signals it is the best form of modulation for dynamic closed loop control [10]. Generally the NS techniques in the past was implemented by using analog devices, nowadays up-to date digital devices are used making possible the accurate implementation of the

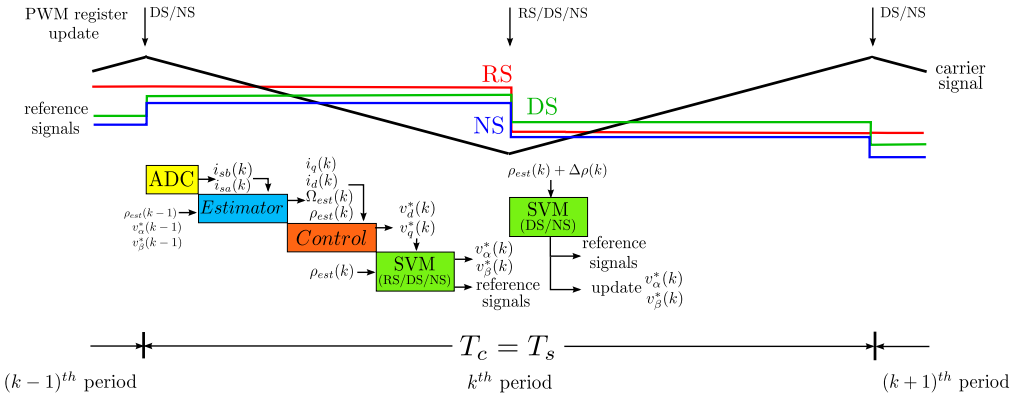

(a) Using shunt resistor

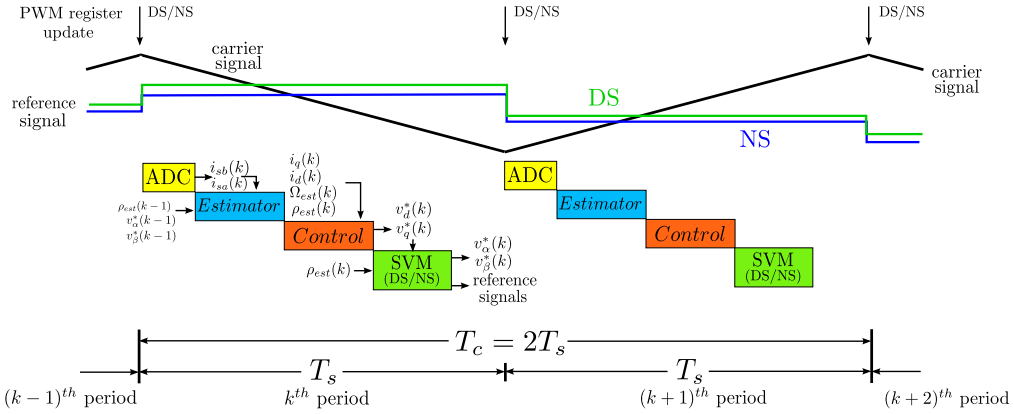

(b) Using current transducer

Fig. 3. Sampling techniques of SVM

NS. In open-loop in most cases the reference signals are multisampled during a carrier signal period by utilizing the parallel computing properties of the FPGA. In closed-loop the multisampling approach requires increasing the sampling frequency as well. The main drawback of this approach is represented by the need for proper filtering of the switching noise from the control signals. Filtering the control signals may impair the system phase margin, reducing the advantage of the multisampling strategy [10].

The first author developed and successfully implemented a digital technique with a sampling rate double of the carrier frequency which is capable to realize accurately the NS technique in open loop [13].

Figure 4 presents the calculation method for the determination of the intersection points of the carrier and the reference signals. Generally the PWM peripheral modules applied in digital devices consist of an up-down counter, a period register (PR) and three compare registers for each phase (CR_i, $(i = a, b, c)$). The triangular carrier curve is approximated by a large number of steps stored in PR (Fig 4). The function is called at the peaks of each carrier signal. As a first step the algorithm calculates the point $v^{**}_{ref,i}$ (or $v^{**}_{ref,j}$) of the theoretical curve (denoted by red line). If the value of point $v^{**}_{ref,i}$ is larger than $PR/2$ then $v^{***}_{ref,i}$ is also calculated and the theoretical curve is approximated by a straight line between $v^{**}_{ref,i}$ and $v^{***}_{ref,i}$. Otherwise, when point $v^{**}_{ref,j}$ is smaller than $PR/2$ the reference value $v^{***}_{ref,i}$ is determined and the theoretical curve is approximated by a straight line between $v^{*}_{ref,j}$ and $v^{**}_{ref,j}$.

By simple mathematical relationships the crossing point can be determined and its value can be latched to the CR_i (or CR_j) register.

The estimator block uses the value of v_α and v_β to calculate the mechanical speed and the flux angle. The exact v^*_α and v^*_β should be recalculated from $v_{ref,i}$ $(i = a, b, c)$ by an inverse Park transformation.

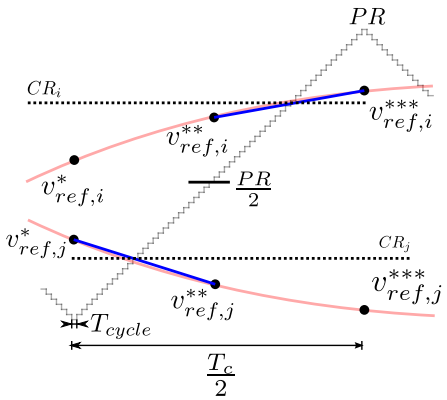

Fig. 4. Algorithm of digitally implemented NS SVM

As it was mentioned the NS technique is advantageous

as it does not introduce distortion or a delayed response. However, in [13] it was verified by simulations and laboratory measurements that the NS SVM technique in open-loop can generate DC voltage in each phase of a three-phase load and its value can be significantly high provided that the ratio of the carrier frequency over the reference frequency m_f is low. Furthermore considerable amount of subharmonic currents and fluxes can be generated by NS SVM when m_f is low and not integer.

B. Sampling of SVM in FOC drive

Later on the effect of the sampling technique of SVM are compared by simulation and laboratory measurements. Depending on the applied current measurement circuit different sampling technique can be implemented.

First shunt current measurement technique is assumed (Fig.3a). In this case all the three SVM sampling techniques can be implemented. The most common solution is the RS [9], [8]. The current sampling takes place at the positive peak of the carrier signal ($T_s = T_c$). After the estimation and the control algorithm the SVM blocks calculates v_α^* and v_β^* and the reference signals $v_{ref,i}$ $(i = a, b, c)$ for each phase. However the calculation takes less time than $T_c/2$ it is advisory to update the registers of the digital PWM module at the beginning of the next sampling period (at the minimum peak of the carrier signal). It indicates a $T_c/2 = T_s/2$ time delay in the control algorithm.

By using DS the accuracy of the SVM algorithm can be improved by recalculating v_α^* and v_β^* and the reference signals $v_{ref,i}$ $(i = a, b, c)$ at the negative peak of the carrier signal. By assuming that Ω_1 is constant over a carrier period the value of the estimated rotor flux angle ρ_{est} at the negative peak of the carrier signal can be approximated as $\rho_{est}(k) + \Delta\rho(k)$ where $\Delta\rho(k) = \frac{\rho_{est}(k)-\rho_{est}(k-1)}{2}$. The calculation takes less time than $T_c/2$ but again the registers of the digital PWM module updated a half period later (at the maximum peak of the carrier signal) resulting again a $T_c/2 = T_s/2$ time delay in the control algorithm (see Fig.3a).

By using the digital NS technique introduced previously the accuracy of SVM can be further improved. By assuming that Ω_1 is constant over a carrier period the value of the estimated rotor flux angle change over one half (to calculate $v_{ref,i}^{***}$ or $v_{ref,j}^{***}$, Fig.4) and one quarter carrier period (to calculate $v_{ref,i}^{**}$ or $v_{ref,j}^{**}$, Fig.4) in k^{th} period are $\Delta\rho_h = \frac{\rho_{est}(k)-\rho_{est}(k-1)}{2}$ and $\Delta\rho_q = \frac{\rho_{est}(k)-\rho_{est}(k-1)}{4}$, respectively.

Again the calculation takes less time than $T_c/2$, but it advisory to update the duty ratio of the digital PWM module only in the next half carrier period. It means that the reference value belonging to the rising edge are calculated during falling edge and vice-versa. Furthermore it results in a $T_c/2 = T_s/2$ time delay in the control algorithm.

Second it is assumed current transducer is applied (Fig3b). By applying current transducer the phase current can be measured continuously. However, as it was explained previously, the stator currents are sampled only at the positive and the negative peaks of the carrier signal ($T_s = 2T_c$) to remove ripples in the current signal or because the digital PWM module enable double update rate. Thus, in this case DS and NS sampling techniques can be applied only.

By using DS the reference signals $v_{ref,i}$ $(i = a, b, c)$ are calculated for each phase at the peaks of the carrier signal. As in this case the estimator block calculates directly ρ_{est} at the negative peak of the carrier signal as well, there is no need for angle approximation as presented previously assuming shunt current measurement technique. Similarly as in the previous cases it is advisory to update the registers of the PWM module in the next half carrier period resulting in a $T_c/2 = T_s$ time delay.

In the case when NS sampling technique is applied, the estimator algorithm is called twice over a carrier frequency, resulting that, by assuming that Ω_1 is constant over a half carrier period, the value of the estimated rotor flux angle change over one half and one quarter carrier period in k^{th} period are $\Delta\rho_h = \rho_{est}(k) - \rho_{est}(k-1)$ and $\Delta\rho_q = \frac{\rho_{est}(k)-\rho_{est}(k-1)}{2}$, respectively.

V. Small Signal Laplace-Domain Analysis

A. Transfer function of SVM process

Assuming RS sampling technique the SVM process introduces a phase lag which can be approximated by a pure delay. As shown in [10], [11], [14]

$$G_{PWM,RS} \approx e^{-s\frac{T_c}{2}} \tag{1}$$

By applying DS, the transfer function of the SVM process is

$$G_{PWM,DS} \approx e^{-s\frac{T_c}{4}} \tag{2}$$

For NS for the phase lag is zero.

B. Small signal analysis of the speed control loop

The previously discussed G_{PWM} transfer function can be used to investigate the effect of the sampling process on the stability of the FOC. The paper focuses on the q axis speed control loop by assuming the d axis flux control loop works properly. Figure 5 shows the block diagram of the speed control loop taking into account the effect of the digital implementation. During the small signal analysis we assume that the estimator discussed previously works properly and the estimated speed is equal to the actual one.

At the beginning of each sampling period the i_{sq}^* reference current signal is calculated from the difference of the estimated and reference speed. The PI controller of the inner current loop calculates the reference v_q^* by using the sampled and transformed signal of the stator phase current. v_q^* is the input reference signal for the PWM inverter. The effect of the Zero-Order Hold (ZOH) at the output of the PI current controller can be given by the following transfer function [10] using the first order Padé-approximation

$$G_{ZOH}(s) \approx \frac{1}{1 + 0.5T_s s} \tag{3}$$

As it was mentioned previously the calculation takes less time than $T_c/2$, but it advisory to update the duty ratio of the

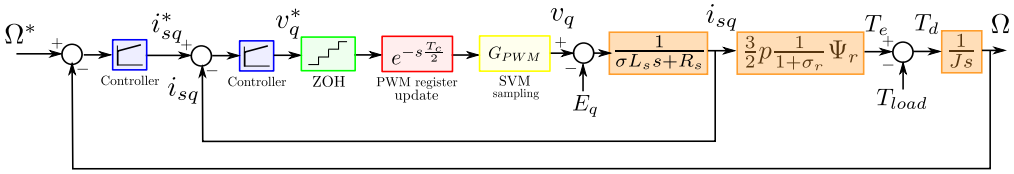

Fig. 5. Block diagram of the q-axis speed control loop taking into account the effect of the digital implementation

digital PWM module only in the next half carrier period. It results in a fixed delay, which can be expressed by $G_{delay} = e^{-s\frac{T_c}{2}}$. By using the first order Padé approximation

$$G_{delay} = e^{-s\frac{T_c}{2}} \approx \frac{1 - \frac{T_c}{4}s}{1 + \frac{T_c}{4}s} \tag{4}$$

Figure 6 shows the Bode diagram of speed control loop shown in Fig.5 (the parameters of the motor and the controllers can be found in Table) both when shunt resistor ($T_c = T_s =$ 1.4 kHz, Fig.6a) and current transducer ($T_s = T_c/2$, Fig.6b) is applied to measure the stator current. During the analysis the E_q BEMF term is omitted and it is assumed the loading torque T_{load} is zero.

Based on the equivalent transfer function and the Bode-plots two main conclusions can be derived

1) The approximated block diagram in Fig.5 takes into account only the effect of $T_c = 1/f_c$ and $T_s = 1/f_s$ and it is not capable to model the effect of the fundamental frequency f_1 and in this way the effect of the carrier to fundamental frequency ratio $m_f = f_c/f_1$ and the sampling to fundamental frequency ratio $F = f_s/f_1$.
2) Based on the phase plots, it can be concluded at the same set of controller parameter the NS sampling technique has the largest phase margin and in this ways its performance are the most robust. By comparing the response of RS and DS, when shunt current measurement technique is assumed, it can be concluded according to Fig.6a it is worth to resample the SVM signal as theoretically a more robust performance can be obtained.

VI. SIMULATION AND EXPERIMENTAL RESULTS

To investigate the effect of the sampling technique of SVM on the operation of vector controlled induction machine drive both simulation and experimental analysis were carried out. The parameters of the motor used both during simulation and laboratory tests can be found in Table I.

The complete simulation model of the speed sensor-less FOC using both shunt resistor and current transducer to measure phase currents was developed in MATLAB Simulink environment with the help of the SimPower Systems toolbox. To make the simulation more realistic the algorithm of the estimator and the controllers were implemented using the Embedded Matlab Function (EMF) block. The script in EMF is practically the same as the C code, which was implemented in the microcontroller. The effect of the time delay caused by the PWM update was also taken into consideration.

TABLE I
Parameters of IM and the inverter

Symbol	Name	Value
P_n	Nominal power	3 kW
n_n	Nominal rated speed	18/24 krpm
f_{1n}	Rated frequency	300 Hz
$V_{LL,rms}$	Nominal voltage	380 V
$I_{ph,rms}$	Nominal current	7.7 A
τ_n	Rated torque	1.5 Nm
R_s	Stator resist.	1.125 Ω
R_r	Rotor resist.	0.85 Ω
L_{ls}	Stator leak. induct.	25 mH
L_{lr}	Rotor leak. induc.	14 mH
L_m	Magnetizin ind.	84.82 Ω
J	Inertia	5 $kgcm^2$

The drive using shunt resistor to measure the phase currents was built and tested in the laboratory. The experiments with the drive using current transducer will be discussed in an other paper. The discrete version of the estimator and the control algorithm was implemented in a dsPIC Digital Signal Controller. In the experimental setup two identical induction machines are mechanically coupled. One runs as the test machine while the other acts as a generating load.

As the analysis focuses on the case when the ratio of sampling frequency over fundamental frequency F is low, it is advisory to use Tustin integration rule instead of the backward Euler method to improve the accuracy of the calculation.

Due to the maximum allowable DC link voltage of the three phase inverter available in the laboratory ($V_{DC} < 400V$) the maximum fundamental frequency was limited to $f_{1max} \approx 160 - 170$ Hz to not operate the motor in field weakening region. Thus the maximum speed is around 10 krpm. To investigate the drive when both the current sampling over reference frequency ratio F and the carrier over reference frequency m_f are low the carrier frequency is reduced. The selected carrier frequencies is quite low compared to the values applied in practical ac drives at the same power level, but in this way the effect of sampling techniques can be emphasized.

To made the results comparable with each other, the same controller parameters were used for all the SVM sampling techniques. The fundamental frequencies are varied to obtain different F and m_f values and f_c and f_s are kept constant. Furthermore the amplitude modulation ratio m_a is also kept constant ($m_a \approx 0.9$) at different reference speed. Thus, the DC link voltage is varied based on the expression $V_{DC} = \frac{2\hat{V}_{ref}}{m_a}$, where $\hat{V}_{ref}$ is the amplitude of the reference voltage at a given fundamental frequency.

First shunt current measurement technique is assumed. The sampling and carrier frequency is $f_s = f_c = 1.4$ kHz. Figure

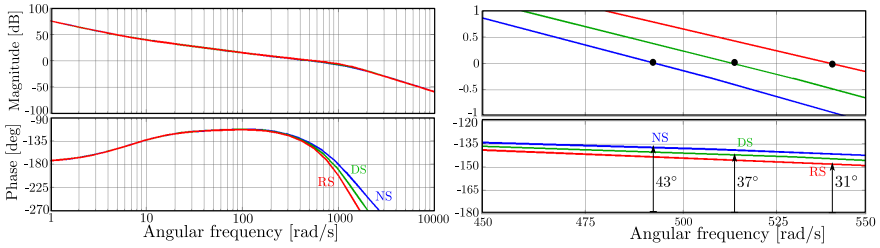

(a) Using shunt resistor, $T_s = T_c$, $f_c = 1.4$ kHz

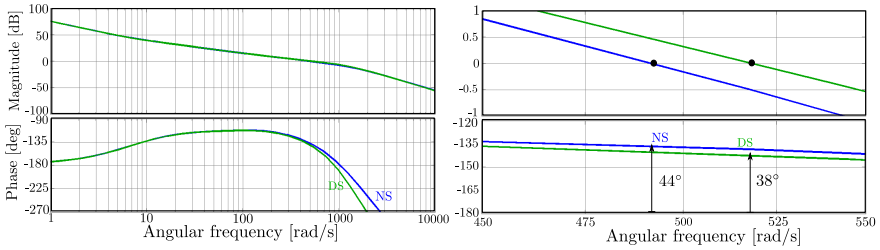

(b) Using current transducer, $T_s = T_c/2$, $f_c = 1.1$ kHz

Fig. 6. Bode plots

7 shows the simulated time function of mechanical speed and the electric torque when $\Omega^* = 440$ rad/s (denoted by dotted line on Fig.7a) ($F = m_f \approx 20$). As it was expected at higher frequency ratios the difference between RS, DS and NS is minimal. Both the time function of the mechanical speed and the electric torque are practically the same. Figure 8 shows the measured stator current vector in steady state. Similar to the simulation results the difference between the three sampling technique is negligible.

By decreasing the sampling (and the carrier) frequency the response of the FOC using RS becomes oscillatory and even unstable. Figure 9a and 9b shows the simulated and measured time function of i_α and i_β for sudden torque change ($\Delta T_{load} = 0.7$ Nm), when $\Omega^* = 1050$ rad/s resulting that $F = m_f = 8.75$. As it can be seen the system becomes unstable after the transient. During the laboratory analysis the over-current protection was activated and it shut down the system to avoid the machines from damages. Figure 9c shows the path of the measured stator current vector when $T_{load} = 0.7$ Nm for DS at the same reference speed. Similar result was obtained for NS. The operation is stable, but the current signal has a high harmonic content due to the low m_f value. By further decreasing the frequency ratio the response of FOC applying DS or NS becomes unstable practically at the same F ratio. Based on the simulation and the experimental results the border of stability is around $F = m_f \approx 8.25$ both for NS and DS for the parameters given in Table .

Based on the simulation and experimental results it can be concluded it is worth to resample the SVM at the negative peak of the carrier signal as more robust control performance can be obtained. However, there is no significant difference between NS and DS.

Second it is assumed current transducer is applied. The sampling and the carrier frequency is $f_s = 2.2$ kHz $f_c = 1.1$ kHz, respectively. According to our analysis, when F and $m_f = F/2$ is a higher value ($F > 20$) there are no significant difference between NS and DS. By decreasing F NS has a more robust performance. Figure 10 shows the simulated time function of mechanical speed and the electric torque when $\Omega^* = 1050$ rad/s (denoted by dotted line on Fig.10) ($F = 2m_f \approx 13.75$). By comparing the response of DS and NS it can be concluded NS has better performance at low pulse

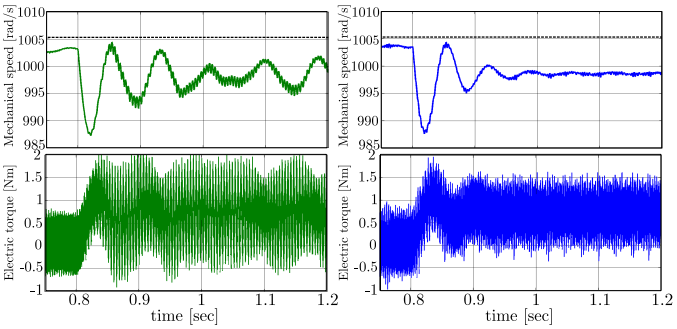

(a) DS (b) NS

Fig. 10. Simulated response for sudden torque change, $\Omega^* = 1050$ rad/s, $F \approx 13.7$, $m_f \approx 6.875$, $\Delta T_{load} = 0.7$ Nm

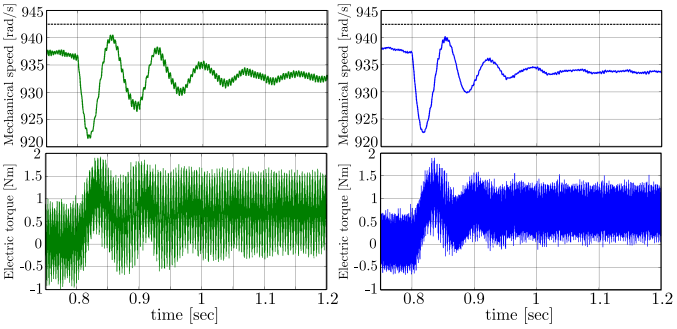

(a) DS (b) NS

Fig. 11. Simulated response for sudden torque change, $\Omega^* = 942$ rad/s, $F \approx 14.6$, $m_f \approx 7.33$, $\Delta T_{load} = 0.7$ Nm

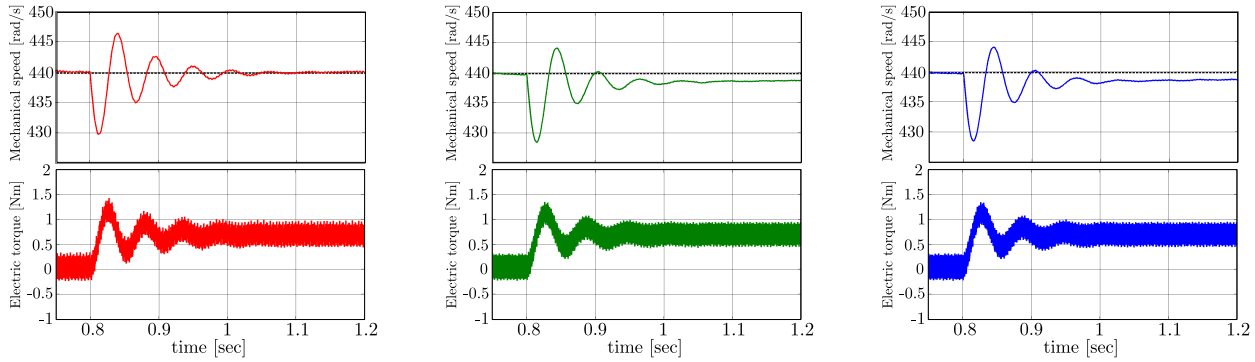

(a) RS (b) DS (c) NS

Fig. 7. Simulated response for sudden torque change, $\Omega^* = 440$ rad/s, $F = m_f \approx 20$, $\Delta T_{load} = 0.7$ Nm

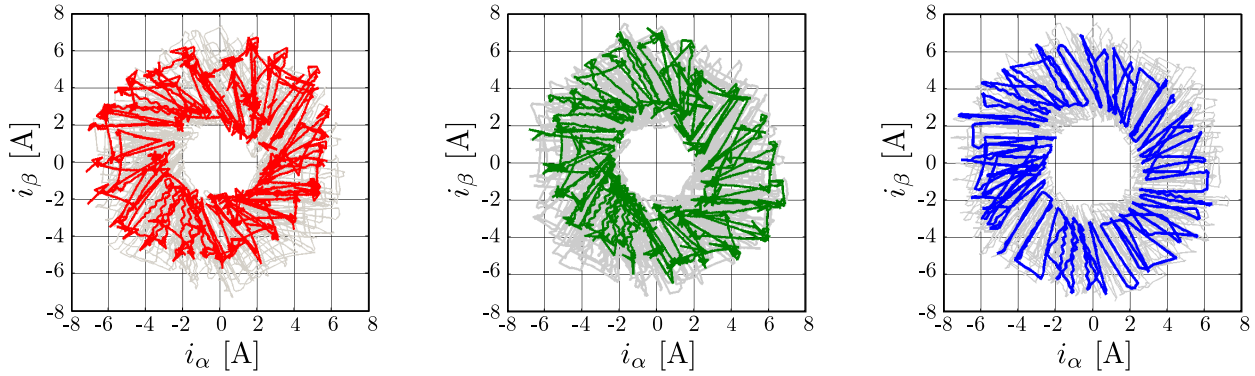

(a) RS (b) DS (c) NS

Fig. 8. Measured stator current vector $\mathbf{i}_s$, $F = m_f \approx 20$, $T_{load} = 0.7$ Nm

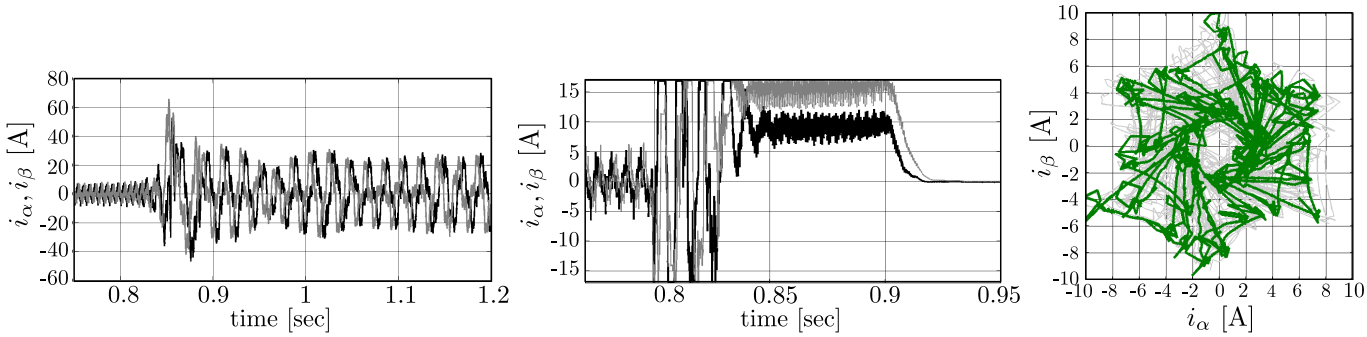

(a) Simulated time function of i_{alpha} and i_β, RS (b) Mesured time function of i_{alpha} and i_β, RS (c) Measured stator current vector $\mathbf{i}_s$, DS

Fig. 9. $\Omega^* = 1050$ rad/s, $F = m_f \approx 8.75$, $T_{load} = 0.7$ Nmm

ratio. The large high frequency torque pulsation generated by DS is unacceptable.

Speed sensor-less FOC control methods must be robust to plant parameter variations. Figure 11 shows the simulated transient responses of the speed control loop for sudden torque change when the L_m mutual inductance value used during the estimation is 20 % smaller than the actual one. The reference speed $\Omega^* = 942$ rad/s ()$F \approx 14.6$, $m_f \approx 7.33$, The simulation results clearly demonstrated that the NS is more robust at low frequency ratios.

Experimental results when current transducer is applied will be presented in another paper.

VII. CONCLUSION

The work described in the paper studied the effect of the implementation form of the Space Vector Modulation (SVM) technique in the operation of an induction machine drive, when speed sensor-less Field Oriented Control (FOC) is applied and the frequency ratio is low. Two current measurement techniques (shunt resistor and current transdrucer) and three SVM sampling form (Regular Sampling RS, Doublesampling

DS and Natural Sampling NS) are compared by simulation and laboratory test.

It was shown, when the stator current sampled only once per carrier period, both NS and DS has a better performance than the RS. In this case the difference between DS and NS is negligible.

It was demonstrated by simulation, when current transducer is applied to measure the stator currents, the digital NS SVM technique developed by the authors enhance the performance of the control loop when the pulse ratio is low even for variations in the motor parameters.

ACKNOWLEDGEMENT

The authors wish to thank the Hungarian Research Fund (OTKA K100275) and the Control Research Group of the Hungarian Academy of Sciences (HAS). This work is connected to the scientific program of the "Development of quality-oriented and harmonized R+D+I strategy and functional model at BME" project. This project is supported by the New Széchenyi Plan (Project ID: TÁMOP-4.2.1/B-09/1/KMR-2010- 0002). The work reported in the paper has been developed in the framework of the project Talent care and cultivation in the scientific workshops of BME project. This project is supported by the grant TÁMOP-4.2.2.B-10/12010-0009.

REFERENCES

[1] D. Gerada, A. Mebarki, N.L. Brown, K.J. Bradley, and C. Gerada. Design aspects of high-speed high-power-density laminated-rotor induction machines. *Industrial Electronics, IEEE Transactions on*, 58(9):4039–4047, 2011.

[2] M.P. Kazmierkowski, L.G. Franquelo, J. Rodriguez, M.A. Perez, and J.I. Leon. High-performance motor drives. *Industrial Electronics Magazine, IEEE*, 5(3):6–26, 2011.

[3] J.S. Yim, S.K. Sul, B.H. Bae, N.R. Patel, and S. Hiti. Modified current control schemes for high-performance permanent-magnet ac drives with low sampling to operating frequency ratio. *Industry Applications, IEEE Transactions on*, 45(2):763–771, 2009.

[4] B. P. McGrath, S. G. Parker, and D. G. Holmes. High performance stationary frame ac current regulation incorporating transport delay compensation. *European Power Electronics and Drives (EPE) Journal*, 22(4):17–24, 2012.

[5] Hongrae Kim, Michael W Degner, Juan M Guerrero, Fernando Briz, and Robert D Lorenz. Discrete-time current regulator design for ac machine drives. *Industry Applications, IEEE Transactions on*, 46(4):1425–1435, 2010.

[6] D.P. Marcetic, I.R. Krcmar, M.A. Gecic, and P.R. Matic. Discrete rotor flux and speed estimators for high speed shaft-sensorless im drives, 2013.

[7] VB Porobic, EM Adzic, and DP Marcetic. Performance evaluation of field angle correction scheme for high speed sensorless im. In *Power Electronics and Motion Control Conference (EPE/PEMC), 2012 15th International*, pages LS4b–1. IEEE, 2012.

[8] N. P. Quang and J-A. Dittrich. *Vector Control of Three-Phase AC Machines, System Development in the Practice*. Springer, 2008.

[9] Cheles M. and Sammoud H. Sensorless field oriented control (foc) of an ac induction motor (acim). *Microchip Technology application note AN1162*, 2010.

[10] Simone Buso and Paolo Mattavelli. Digital control in power electronics. *Lectures on Power Electronics*, 1(1):1–158, 2006.

[11] Luca Corradini, Walter Stefanutti, and Paolo Mattavelli. Analysis of multisampled current control for active filters. *Industry Applications, IEEE Transactions on*, 44(6):1785–1794, 2008.

[12] Michael Hornkamp and R Tschirbs. Current shunt resistors integrated in igbt power modules for medium power drive application. *PCIM China. Eupec GmbH*, 2004.

[13] Peter Stumpf, Rafael K Jardan, and Istvan Nagy. Dc components and subharmonics generated by naturally sampled pwm techniques. In *IECON 2012-38th Annual Conference on IEEE Industrial Electronics Society*, pages 327–332. IEEE, 2012.

[14] David M Van de Sype, Koen De Gussemé, Alex P Van den Bossche, and Jan A Melkebeek. Small-signal laplace-domain analysis of uniformly-sampled pulse-width modulators. In *Power Electronics Specialists Conference, 2004. PESC 04. 2004 IEEE 35th Annual*, volume 6, pages 4292–4298. IEEE, 2004.